Viterbi Detection of PSK Signals in Markov Impulsive Noise

Ahmed Mahmood and Mandar Chitre
Acoustic Research Laboratory, Tropical Marine Science Institute, National University of Singapore
e-mail: {ahmed, mandar}@arl.nus.edu.sg

***Abstract*—The ambient soundscape in warm shallow waters is dominated by snapping shrimp noise at frequencies greater than 2 kHz. The noise process is impulsive and exhibits memory. Within the human audible range, this manifests as a persistent background crackle, akin to the popping of corn. Unless catered for, underwater acoustic communication systems are vulnerable to large drops in error performance in such waters. With the advent of new effective statistical models, namely the α-sub-Gaussian noise model with memory order m (αSGN(m)), it is now possible to mitigate snapping shrimp noise by exploiting the latter's temporal amplitude statistics. In our work, we accomplish this by deriving the passband Viterbi algorithm (VA) for a single-carrier scheme in αSGN(m). The results are compared to the symbol-by-symbol maximum-likelihood (ML) detector and conventional L_2-norm detection in scenarios representative of severe snapping shrimp noise. As the VA algorithm is optimal in αSGN(m), it is of much interest to know how it fairs in snapping shrimp noise. This is investigated in our work.**

I. Introduction

In warm shallow waters, snapping shrimp noise is known to be the dominant source of ambient noise at frequencies over 2 kHz [1], [2]. The soundscape offers a unique experience to divers who tend to hear constant crackling (similar to popping corn) in the background. Statistically, the noise exhibits heavy-tailed (non-Gaussian) characteristics and can potentially decimate the performance of acoustic systems operating within [3]. Recorded noise observations exhibit large outliers with peak-to-peak levels surging as high as 190 dB at 1 m [1], [4]. Snapping shrimp noise is indeed a phenomenon unique to warm shallow waters. However, its large global spread poses an unavoidable problem to underwater acoustic systems.

In the literature, several statistical noise models have been developed to characterize snapping shrimp noise [1], [2], [5]. Of these, the stationary α-sub-Gaussian noise with memory order m (αSGN(m)) is arguably the most effective in encapsulating these characteristics for a single hydrophone receiver [5]. Rather than develop a forward noise model based upon the channel, snap rate and spatial distribution of the snapping shrimp, the authors employed a data-driven approach that investigated the temporal amplitude statistics of the recorded noise samples. Outliers in snapping shrimp noise tend to cluster together to form bursts. The noise process thus depicts memory and is essentially *bursty* as well as *impulsive* [5]. The αSGN(m) model tries to characterize these statistics by employing a sliding-window framework and multivariate heavy-tailed α-sub-Gaussian (αSG) distributions. This essentially results in a Markov process of memory order m. The model has found tremendous applicability in the realm of signal processing and communications, which has lead to the construction of ever-more effective algorithms in snapping shrimp noise [6]–[8].

The Viterbi algorithm (VA) [9] has long been employed in communications and essentially computes the maximum-likelihood (ML) of a sequence of symbols from the received observations. Its applicability in the realm of forward error correction has especially garnered a lot of interest over the last few decades [10]. In our work, we derive the VA's branch (and path) metrics for αSGN(m) and test its optimality in several impulsive scenarios. Due to its Markov property, the αSGN(m) naturally fits into the VA framework. However, there are other constraints that need to be adhered to if one is to truly exploit the characteristics of αSGN(m). These are detailed later on in the text.

The contributions of this work are the following: The problem we try addressing is that of optimally detecting transmitted symbols in snapping shrimp noise. To achieve this end, we derive and analyze the performance of the *passband* Viterbi detector in αSGN(m) for a single-carrier communication system. Though our analysis is directed towards phase-shift keying (PSK), it can be extended to other constellation schemes as well. Working with passband samples is key here as conventional (linear) baseband conversion is known to substantially degrade performance in αSGN(0), i.e., impulsive noise with independent and identically distributed (IID) samples [3], [11]. The error performance of the VA is then compared to the symbol-by-symbol passband ML detector derived in [12], [13]. Furthermore, comparisons are also made with the conventional (L_2-norm) detector (applied after linear baseband conversion) [10]. We compute the error performance of each detector in αSGN(m) for different m. Moreover, we also analyze the error performance in practical snapping shrimp noise. This is achieved by tuning the αSGN(m) model to actual snapping shrimp noise datasets and using the estimated parameters within the receiver's framework. As the highlighted detectors offer different levels of optimality in αSGN(m) (and by extension snapping shrimp noise), it is of much interest to quantify their relative performance in realistic settings.

This paper is organized as follows: In Section II, we discuss the forward passband model and briefly introduce the αSGN(m) process. This is followed up by a summary of select contemporary detectors in Section III. We present our derivation of the passband αSGN(m)-based VA in Section IV and discuss our simulation results in Section V. Finally, we wrap up by offering our conclusions in Section VI.

II. Fundamental Concepts

A. The Forward Model

Let x represent a symbol in a phase-shift keying (PSK) constellation of size M, i.e., $x \in \{x_1, x_2, \dots x_M\}$, where $x_k = \sqrt{\mathcal{E}}\exp(j2\pi k/M)$, $\mathcal{E}$ is the transmitted signal energy and $j = \sqrt{-1}$. Then given a symbol time-period of T, the transmitted passband signal can be expressed as

$$s_p(t) = \Re\Big\{x\sqrt{\frac{2}{\bar{\mathcal{E}}_g}}g(t)\exp\Big(j2\pi f_c t\Big)\Big\}, \tag{1}$$

where $g(t) \in \mathbb{R}$ is the baseband shaping pulse, $\bar{\mathcal{E}}_g$ is its *energy* and f_c is the carrier frequency [10]. To maintain an integer number of carrier cycles within each symbol interval, we constrain f_c to be a multiple of $1/T$, i.e., $f_c = \xi/T$ for some $\xi \in \mathbb{Z}^+$. In underwater acoustics, transmit frequencies are limited to a few tens of kilohertz [14]. Therefore, it is possible to sample the passband signal directly. If f_s is the passband sampling frequency, then by ensuring $f_s = N/T$ such that $N \in \mathbb{Z}^+$ we get an integer number of samples per symbol transmission. We observe that f_s needs to satisfy the Nyquist rate, i.e., $f_s > 2(f_c + \frac{\beta}{T})$. Here $\beta \in \mathbb{R}^+$ is the excess bandwidth (roll-off) factor and depends on the choice of $g(t)$ [10].

On invoking the aforementioned conditions, (1) can be discretized and normalized by $\sqrt{f_s}$ to get

$$s[n] = \frac{s_p(\frac{n}{f_s})}{\sqrt{f_s}} = \Re\Big\{x\underbrace{\sqrt{\frac{2}{\mathcal{E}_g}}g[n]\exp\Big(j2\pi\frac{\xi}{N}n\Big)}_{\ell[n]}\Big\}, \tag{2}$$

where $\mathcal{E}_g = \bar{\mathcal{E}}_g f_s$. The discrete passband transmit-receive equation is given by

$$r[n] = s[n] + w[n], \tag{3}$$

where $r[n]$ and $w[n]$ are the received and noise samples, respectively. We have used the square bracket notation to signify discrete-time signals, i.e., $g[n] = g(n/f_s)$ and so on. We observe that $\ell[n]$ can be written in terms of its real and imaginary components, i.e., $\ell[n] = \ell_I[n] + j\ell_Q[n]$, where

$$\ell_I[n] = \sqrt{\frac{2}{\mathcal{E}_g}}g[n]\cos\Big(2\pi\frac{\xi}{N}n\Big) \quad \text{and} \tag{4}$$

$$\ell_Q[n] = -\sqrt{\frac{2}{\mathcal{E}_g}}g[n]\sin\Big(2\pi\frac{\xi}{N}n\Big). \tag{5}$$

As a final note, we see that $\ell_I[n]$ and $\ell_Q[n]$ form an orthonormal basis over the samples $n \in \{0, 1, \dots, N-1\}$, i.e.,

$$\sum_{n=0}^{N-1}\ell_I^2[n] = \sum_{n=0}^{N-1}\ell_Q^2[n] = 1 \quad \text{and} \quad \sum_{n=0}^{N-1}\ell_I[n]\ell_Q[n] = 0.$$

B. The αSGN(m) Model

The αSGN(m) process is based on a sliding-window framework and constrains any adjacent $m+1$ samples to follow a multivariate αSG distribution [5], [8]. More precisely, let $W_n \in \mathbb{R}$ denote a random sample of αSGN(m) at time index n. Then $\vec{W}_{n,m} = [W_{n-m}, W_{n-m+1}, \dots W_n]^\mathsf{T}$ is an $(m+1)$-dimensional αSG distributed random vector and can be expressed as

$$\vec{W}_{n,m} = A_n^{1/2}\vec{G}_{n,m}. \tag{6}$$

Here $\vec{G}_{n,m} = [G_{n-m}, G_{n-m+1}, \dots G_n]^\mathsf{T}$ is a zero-mean Gaussian random vector with covariance matrix $\mathbf{R}_m$, i.e., $\vec{G}_{n,m} \sim \mathcal{N}(\mathbf{0}, \mathbf{R}_m)$ [15], [16]. Moreover, A_n is independent of $\vec{G}_{n,m}$ and is a totally right-skewed stable random variable such that $A_n \sim \mathcal{S}(\frac{\alpha}{2}, 1, 2(\cos(\frac{\pi\alpha}{4}))^{2/\alpha}, 0)$. A stable random variable is parameterized by four parameters, namely, the characteristic exponent $\alpha \in (0, 2]$, the skew $\beta \in [-1, +1]$, the scale $\delta \in \mathbb{R}^+$ and the location $\mu \in \mathbb{R}$ [15]. The corresponding distribution can thus be expressed succinctly as $\mathcal{S}(\alpha, \beta, \delta, \mu)$. We highlight that α uniquely determines the degree of heaviness of the stable distribution. The larger the value of α, the lower the heaviness of the tails of the resulting distribution [15]. As a limiting case, we note that $\mathcal{S}(\alpha, \beta, \delta, \mu) \sim \mathcal{N}(\mu, 2\delta^2)$, thus implying that the Gaussian distribution is a member of the stable distribution family.

As αSGN(m) is a stationary process, $\mathbf{R}_m$ does not vary with time [5] and is essentially a symmetric Toeplitz matrix. From (6), we note that αSGN(m) is a Markov process of order m. This stems from the fact that the distribution of W_n conditional on all previous samples is equivalent to its distribution conditional on the immediately previous m samples, i.e., $\{W_{n-m}, W_{n-m+1}, \dots, W_{n-1}\}$. From the discussion above we note that α and $\mathbf{R}_m$ alone are sufficient to parameterize the αSGN(m) process. Equivalently, by defining the normalized covariance matrix $\acute{\mathbf{R}}_m = \mathbf{R}_m/\delta^2$, αSGN(m) can be conveniently parameterized by α, δ and $\acute{\mathbf{R}}_m$. For a more rigorous approach on αSGN(m), the reader is referred to [8], while [15]–[17] offer great insights in to the workings of αSG and stable distribution theory.

III. Robust and Conventional Detection

We will now briefly comment on the conventional and symbol-by-symbol passband ML detector in αSGN(m). These will be used to benchmark the VA's performance later on in our simulations.

A. The L_2-norm Detector

In the literature, $w[n]$ is typically assumed to be a realization of a Gaussian noise process [10]. In the case of white Gaussian noise (WGN), the optimal detector for the forward model in (3) is based on using the orthonormal basis in (4) and (5) to generate the noisy constellation symbol. This is then given as an input to the L_2-norm (Euclidean) detector [10]. Mathematically, we have

$$r = x + w, \tag{7}$$

where $r = \sum_{n=0}^{N-1} r[n]\ell^*[n]$ and $w = \sum_{n=0}^{N-1} w[n]\ell^*[n]$. A decision on the received symbol is made via the metric

$$\hat{x} = \underset{\mu\in\mathbb{M}}{\texttt{arg min}}\|r - \mu\|^2, \tag{8}$$

where $\mathbb{M}$ represents the set of all (complex) constellation points and $\|\cdot\|$ denotes the L_2-norm.

Do note that the transition from (3) to (7) essentially represents *linear* baseband conversion, a process that is known to be sub-optimal in impulsive noise [3], [11]. The latter fact motivates employing a passband detector to achieve robustness with respect to the noise process. With this in mind, we discuss the passband symbol-by-symbol ML detector next. This has been employed with a fair amount of success in the literature to mitigate the impact of αSGN(m) and snapping shrimp noise in a communications setting [12], [13].

B. Symbol-by-Symbol ML Detection in αSGN(m)

Without any loss of generality, we focus on the first signaling interval in (3), i.e., the samples corresponding to $n \in \{0, 1, \ldots, N-1\}$. Let us define the N-dimensional random vector $\vec{W}_N$, whose sample outcome is the noise vector $\mathbf{w}_N = [w[0], w[1], \ldots, w[N-1]]^{\mathsf{T}}$. We denote the corresponding N-dimensional joint probability density function (PDF) by $f(\mathbf{w}_N)$ and note that this extends to any immediately adjacent N samples in αSGN(m) due to the latter's stationarity. In any case, using the chain rule of probability and the Markovity of αSGN(m), the PDF can be expressed as the following:

$$\begin{aligned} f(\mathbf{w}_N) &= f(\mathbf{w}_m) \prod_{n=m}^{N-1} f(w_n|\mathbf{w}_n), \\ &= f(\mathbf{w}_m) \prod_{n=m}^{N-1} f(w_n|\mathbf{w}_{n-1,m-1}), \\ &= f(\mathbf{w}_m) \prod_{n=m}^{N-1} \frac{f(\mathbf{w}_{n,m})}{f(\mathbf{w}_{n-1,m-1})}. \end{aligned} \tag{9}$$

Here $\mathbf{w}_{n,m} = [w[n-m], w[n-m+1], \ldots, w[n]]^{\mathsf{T}}$ is an $(m+1)$-dimensional vector and $f(\mathbf{w}_{n,m})$ denotes its PDF. We note that $f(\mathbf{w}_{n,m})$ and $f(\mathbf{w}_m)$ are both $(m+1)$-dimensional αSG PDFs, while $f(\mathbf{w}_{n-1,m-1})$ is an m-dimensional αSG PDF [8], [18]. The latter statement stems from the fact that any marginal distribution of a larger dimensional αSG distribution is also αSG [16].

The passband symbol-by-symbol ML detector is given by

$$\hat{x} = \underset{\mu \in \mathbb{M}}{\texttt{argmin}} \; -\log f_{\vec{W}_N}(\mathbf{r} - \mu_I \boldsymbol{\ell}_I - \mu_Q \boldsymbol{\ell}_Q), \tag{10}$$

where $\mathbf{r}$, $\boldsymbol{\ell}_I$ and $\boldsymbol{\ell}_Q$ are vectorized versions of the samples $r[n]$, $\ell_I[n]$, and $\ell_Q[n]$, respectively, for $n \in \{0, 1, \ldots, N\}$. Using (9), one can compute the cost in (10) via successive calls to the elementary αSG distributions. Each call can be computed numerically by the methodologies explained in [16] or [18].

Do note that the form in (10) hints at $N \geq m$. Though this is not a constraint when evaluating (10), it is useful to understand the relationship between these variables in a practical context. When αSGN(m) is tuned to snapping shrimp datasets, m typically results in a small value. For example, $m \in \{4, 5, \ldots, 8\}$ is sufficient to characterize snapping shrimp noise sampled at 180 kHz [7], [8]. If the $N \geq m$ condition is met, then the signal bandwidth B needs to be constrained to $B \leq f_s/m$, which for $m = 4$ is $B \leq 45$ kHz and for $m = 8$ is $B \leq 22.5$ kHz. Consequently, $N \geq m$ holds true when B spans a few tens of kHz, which is the case for most contemporary underwater acoustic modems [19].

In the next section, we derive the VA's branch and path metrics for αSGN(m). As we shall see, the latter's Markov property allows convenient mathematical tractability and offers a natural fit into the VA's framework.

IV. ML Sequence Detection in αSGN(m)

The αSGN(m) process is one that exhibits memory. Therefore the optimal detector should be able to exploit the dependency amongst noise samples. In this sense, the ML symbol-by-symbol detector discussed in Section III-B is sub-optimal. However, we note that the ML *sequence* detector is optimal in this regard. Such schemes may offer key advantages as dependence amongst the noise samples may be spread over several adjacent symbol intervals in a single-carrier system. In practice, the average duration of a single snap in snapping noise is observed to be on the order of 2 milliseconds [20]. Therefore, a snap may impact several adjacent signaling intervals if data rates on the order of several kilohertz are required.

Due to αSGN(m) being Markov, the ML sequence detector latter is computed efficiently by the VA. As highlighted before, linear processing in the presence of impulsive noise is sub-optimal [3]. Therefore, to avoid this, we derive the VA directly for the passband signal. Thus, the VA is used not only as a detector but also as a robust baseband conversion block.

Now that we want to derive the ML sequence detector, the signaling interval needs to be incorporated in our derivation. Let L be the total number of transmitted symbols. Then with N samples per transmitted symbol, the joint-PDF of any adjacent LN samples can be expressed as

$$\begin{aligned} f_{\vec{W}}(\mathbf{w}_{LN}) &= f(\mathbf{w}_m) \prod_{n=m}^{LN-1} f(w_n|\mathbf{w}_{n-1,m-1}), \\ &= f(\mathbf{w}_N) \prod_{i=2}^{L} \prod_{n=(i-1)N}^{iN-1} f(w_n|\mathbf{w}_{n-1,m-1}), \\ &= f(\mathbf{w}_N) \prod_{i=2}^{L} \prod_{n=(i-1)N}^{iN-1} \frac{f(\mathbf{w}_{n,m})}{f(\mathbf{w}_{n-1,m-1})}, \end{aligned} \tag{11}$$

where i indexes the signaling interval for the i^{th} transmitted symbol. Due to the Markovity of αSGN(m), the noise samples at $n \in \{(i-1)N - m + 1, \ldots, (i-1)N\}$ are dependent on the noise samples within the i^{th} signaling interval. However, unlike (10), the form in (11) allows exploiting this dependence between different signaling intervals.

The ML sequence estimate of the transmitted symbols boils down to maximizing (11) with respect to the L transmitted symbols. From the perspective of the VA, we observe from (11), that state transitions occur at the end of every signaling interval, i.e., after every N samples. Moreover, denoting the p^{th} state at signaling interval i as $S_p(i)$, we note that the latter can be defined as a set of $\lceil m/N \rceil$ constellation symbols encountered within the intervals $\{i - \lceil m/N \rceil + 1, i - \lceil m/N \rceil + 2, \ldots, i\}$. Consequently, as M is the employed constellation size, the resulting state space is of cardinality $M^{\lceil m/N \rceil}$. As highlighted in Section III-B, the constraint $N \geq m$ represents a realistic scenario in a contemporary underwater acoustic

communications receiver. In this case, the state space is limited to size M and $S_p(i) = \{x_p\}$. Using this as our scenario of interest (and with a slight abuse of notation), we assume a *known* symbol for the $i = -1$ signaling interval. Consequently, from (11), we have

$$f_{\vec{W}}(\mathbf{w}_{LN}) = \prod_{i=1}^{L} \prod_{n=(i-1)N}^{iN-1} \frac{f(\mathbf{w}_{n,m})}{f(\mathbf{w}_{n-1,m-1})}, \tag{12}$$

which after taking the logarithm becomes

$$\log f_{\vec{W}}(\mathbf{w}_{LN}) = \sum_{i=1}^{L} \underbrace{\left(\sum_{n=(i-1)N}^{iN-1} \log \frac{f(\mathbf{w}_{n,m})}{f(\mathbf{w}_{n-1,m-1})} \right)}_{\Rightarrow\ \gamma_{p,q}(i)\ \triangleq\ \gamma(S_p(i-1),S_q(i))}. \tag{13}$$

We denote the branch metric between $S_p(i-1)$ and $S_q(i)$ by $\gamma_{p,q}(i) \triangleq \gamma(S_p(i-1), S_q(i))$ and note it to be based on the summing terms within the parenthesis in (13). Moreover, the outer sum contributes to the weight of the overall path. To be precise, let us define

$$v_n^{(i,p,q)} = \begin{cases} \Re\{x_q \ell[n]\} & \text{if } n \geq (i-1)N \\ \Re\{x_p \ell[n]\} & \text{if } n < (i-1)N \end{cases} \tag{14}$$

and the vector $\mathbf{v}_{n,m}^{(i,p,q)} = [v_{n-m}^{(i,p,q)}, v_{n-m+1}^{(i,p,q)}, \ldots v_n^{(i,p,q)}]^{\mathsf{T}}$. Then with obvious notation we have the following expression for the branch metric:

$$\gamma_{p,q}(i) = -\sum_{n=(i-1)N}^{iN-1} \log \frac{f(\mathbf{r}_{n,m} - \mathbf{v}_{n,m}^{(i,p,q)})}{f(\mathbf{r}_{n-1,m-1} - \mathbf{v}_{n-1,m-1}^{(i,p,q)})}. \tag{15}$$

The VA algorithm computes $\gamma_{p,q}(i)$ in (15) for every possible $S_p(i-1) \rightarrow S_q(i)$ transition at the i^{th} step in the trellis. Based on the accumulative cost (path metric) of successive transitions, certain paths can either be discarded or retained for future use [9], [10]. State transitions that maximize $\sum_{i=1}^{L} \gamma_{p,q}(i)$ are eventually chosen and from it the estimated data vector $\hat{\mathbf{x}}$ is discerned. In Fig. 1, we highlight the potential paths for the i^{th} signaling interval. The branch metrics for each edge in the trellis are also shown. Do note that the corresponding Markov chain is fully connected, i.e., given any starting state, the probability of ending up in any other state within a single transition is non-zero.

With the branch metrics and state space sufficiently defined for the αSGN(m)-based VA, we present our results next.

V. Simulation Results

For our simulations, we first tune the αSGN(m) model to ambient noise observations sampled at 180 kHz in Singapore coastal waters. The latter offers a thriving climate for the snapping shrimp [2]. Consequently, the noise within is non-Gaussian and offers a great opportunity to test the effectiveness of the αSGN(m)-based VA. Do note that as $\acute{\mathbf{R}}_m$ can be completely constructed from its first row, we list down the latter's estimates in Table I for a maximum order of $m = 8$. For all our simulations, we employ $f_c = 36$ kHz and $1/T = 18$ kHz, which results in $\xi = 2$ and $N = 10$. For the VA, we set $L = 10000$ for each Monte Carlo

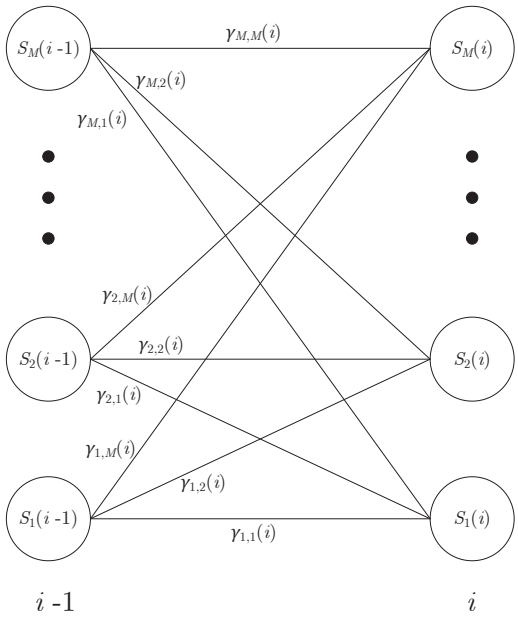

Fig. 1. Transitions between states within the trellis for the i^{th} signaling interval.

TABLE I
$\acute{r}_{1j}$ FROM SNAPPING SHRIMP NOISE SAMPLED AT 180 KHZ.

j	$\acute{r}_{1j}$
1	1.000
2	0.662
3	0.308
4	0.182
5	0.045
6	0.029
7	0.018
8	-0.038
9	-0.103

iteration. Our simulation setup focuses on evaluating the bit error rate (BER) and symbol error rate (SER) performance of binary PSK (BPSK) and quadrature PSK (QPSK), respectively, in αSGN(m) and recorded observations of snapping shrimp noise. The BER/SER is plotted against a signal-to-noise ratio (SNR) measure, which is defined as

$$\text{SNR} = \frac{\mathcal{E}}{4\delta^2 \log_2 M}, \tag{16}$$

where δ is the scale parameter of the noise samples in (3). Finally, error performance in αSGN(m) is determined for $\alpha = 1.5$, as this is representative of severe snapping shrimp noise [1], [2].

In Figs. 2 & 3, we present the BER and SER performance of BPSK and QPSK, respectively, in αSGN(4). The VA results are compared to that of the symbol-by-symbol ML

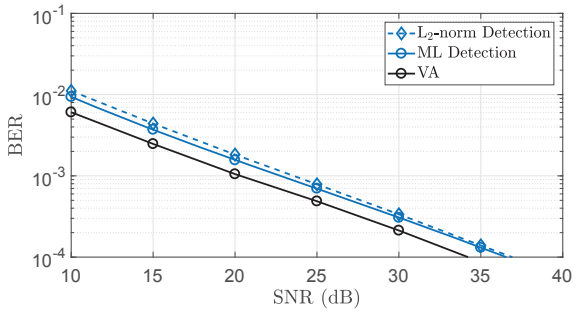

Fig. 2. Performance comparison of BPSK in αSGN(4) for $N = 10$.

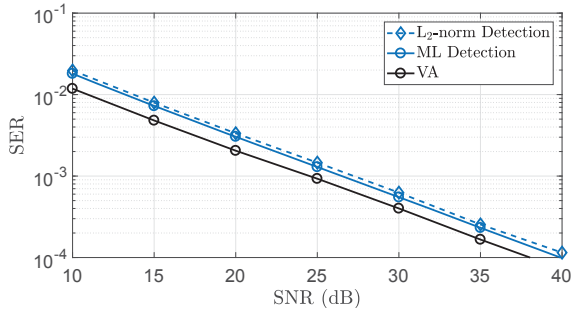

Fig. 3. Performance comparison of QPSK in αSGN(4) for $N = 10$.

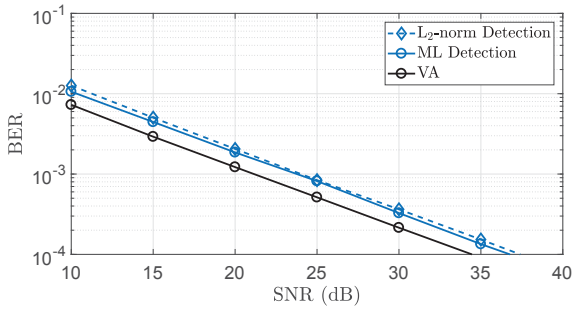

Fig. 4. Performance comparison of BPSK in αSGN(8) for $N = 10$.

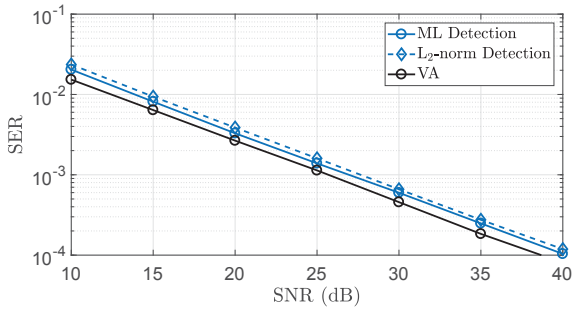

Fig. 5. Performance comparison of QPSK in αSGN(8) for $N = 10$.

detector (applied directly to the passband samples) and also to the conventional L_2-norm Euclidean detector. In either plot, the VA offers approximately 2.5 dB improvement over the conventional approach at error rates of 10^{-4}. We observe similar trends in Figs. 4 & 5, where we plot the BER and SER performance of BPSK and QPSK, respectively, in αSGN(8). One also observes a *slight* degradation in error performance between the $m = 4$ and $m = 8$ cases. This is due to the fact that an impulse is retained over a relatively larger number of samples for αSGN(8) and can potentially impact more of the transmitted symbols.

In Figs. 6 & 7, we analyze the performance of the αSGN(m)-based VA in recorded samples of snapping shrimp noise for BPSK and QPSK, respectively. The VA detector assumes a memory order of $m = 4$ for computing the elementary αSG PDFs of $\gamma_{p,q}(i)$ in (15). Also plotted are the error performances of the symbol-by-symbol ML detector and the L_2-norm detector. Our considered snapping shrimp dataset offers less impulsiveness ($\alpha = 1.57$) than the simulation settings of Figs. 2–5, which results in the overall better performance of all detectors. However, we note that the VA still clearly outperforms the conventional detector by around 3 dB at an error rate of 10^{-4} for both BPSK and QPSK.

Being optimal in the ML sense, it is of no surprise that the VA outperforms other detection schemes. However, the 2.5–3.0 dB improvement it offers is a significant margin. This is particularly attractive as we maintain a unit coding rate. Nevertheless, we note that the over all performance of the considered detectors is still not desirable as they all require several tens of decibels worth of SNR to achieve good error performance (SER, BER$\leq 10^{-4}$). This is directly attributed to the high-rate uncoded single-carrier setup employed in our

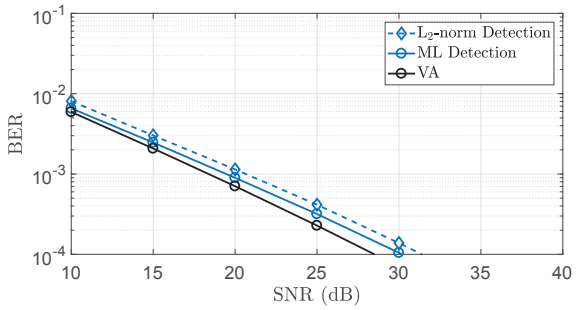

Fig. 6. Comparison of BPSK in snapping shrimp noise for $N = 10$.

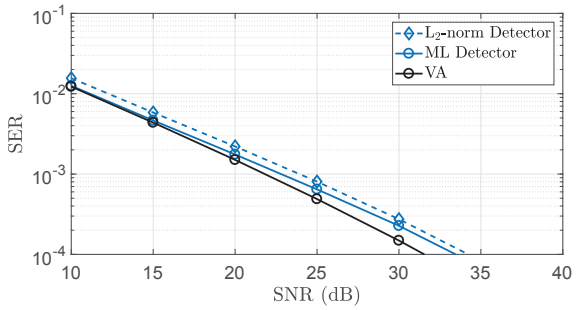

Fig. 7. Comparison of QPSK in snapping shrimp noise for $N = 10$.

work. For this scenario, a single burst may impact entire signaling intervals (and more), leaving absolutely no part of the signal free from the contamination. Though the VA algorithm alleviates its effect, the overall simulation setup is the bottleneck that primarily hinders performance. This can be avoided by incorporating the VA within a convolutional or turbo coded high-rate single-carrier system, which allows

spreading of a transmitted symbol's energy over a duration larger than that of an average snap. Such avenues allow interesting opportunities for future research in the realm of acoustic communications in snapping shrimp noise.

VI. Conclusion

We derived the branch and path metrics of the VA for passband αSGN(m). The latter is an efficient model for snapping shrimp noise, which in turn is abundantly observed in warm shallow waters. Detection performance was evaluated for BPSK and QPSK in αSGN(4) and αSGN(8). Parameters of the αSGN(m) process were initially tuned to actual snapping shrimp noise datasets. In all cases, the VA was shown to outperform the symbol-by-symbol ML detector (applied to the passband samples) and the L_2-norm detector (after linear baseband conversion). The same schemes were then analyzed in actual snapping shrimp noise, which exhibited similar trends. Our findings highlighted that the αSGN(m)-based VA presented a suitable choice for a robust detector in a single-carrier underwater acoustic system. However, it is presumed to be best used in conjunction with convolutional/turbo codes, where the energy of a symbol can be distributed over intervals longer than the average snap (burst) length.

References

[1] M. W. Legg, "Non-Gaussian and non-homogeneous Poisson models of snapping shrimp noise," Ph.D. dissertation, Curtin Univ. of Technology, 2009.

[2] M. Chitre, J. Potter, and S.-H. Ong, "Optimal and near-optimal signal detection in snapping shrimp dominated ambient noise," *IEEE J. Ocean. Eng.*, vol. 31, no. 2, pp. 497 –503, April 2006.

[3] A. Mahmood, "Digital communications in additive white symmetric alpha-stable noise," Ph.D. dissertation, Natl. Univ. of Singapore, June 2014.

[4] W. W. L. Au and K. Banks, "The acoustics of the snapping shrimp synalpheus parneomeris in kaneohe bay," *The J. of the Acoustical Soc. of Amer.*, vol. 103, no. 1, pp. 41–47, 1998.

[5] A. Mahmood and M. Chitre, "Modeling colored impulsive noise by Markov chains and alpha-stable processes," in *MTS/IEEE Oceans - Genoa, 2015*, May 2015, pp. 1–7.

[6] A. Mahmood, H. Vishnu, and M. Chitre, "Model-based signal detection in snapping shrimp noise," in *2016 IEEE Third Underwater Commun. and Networking Conf. (UComms)*, Aug 2016, pp. 1–5.

[7] A. Mahmood and M. Chitre, "Optimal and near-optimal detection in bursty impulsive noise," *IEEE J. Ocean. Eng.*, vol. PP, no. 99, pp. 1–15, 2016.

[8] A. Mahmood, M. Chitre, and H. Vishnu, "Locally optimal inspired detection in snapping shrimp noise," *IEEE J. Ocean. Eng.*, vol. 42, no. 4, pp. 1049–1062, Oct 2017.

[9] A. Viterbi, "Error bounds for convolutional codes and an asymptotically optimum decoding algorithm," *IEEE Trans. Inf. Theory*, vol. 13, no. 2, pp. 260–269, April 1967.

[10] J. Proakis and M. Salehi, *Digital Communications*, ser. McGraw-Hill higher education. McGraw-Hill Education, 2007.

[11] A. Mahmood, M. Chitre, and M. A. Armand, "On single-carrier communication in additive white symmetric alpha-stable noise," *IEEE Trans. Commun.*, vol. 62, no. 10, pp. 3584–3599, Oct 2014.

[12] A. Mahmood and M. Chitre, "Uncoded acoustic communication in shallow waters with bursty impulsive noise," in *2016 IEEE Third Underwater Commun.and Networking Conf. (UComms)*, Aug 2016, pp. 1–5.

[13] ——, "Robust communication in bursty impulsive noise and rayleigh block fading," in *Proc. of the 11th ACM Int. Conf. on Underwater Networks & Systems*, ser. WUWNet '16. New York, NY, USA: ACM, 2016, pp. 13:1–13:7. [Online]. Available: http://doi.acm.org/10.1145/2999504.3001111

[14] M. Stojanovic and J. Preisig, "Underwater acoustic communication channels: Propagation models and statistical characterization," *IEEE Commun. Mag.*, vol. 47, no. 1, pp. 84–89, January 2009.

[15] G. Samorodnitsky and M. S. Taqqu, *Stable Non-Gaussian Random Processes: Stochastic Models with Infinite Variance*. Chapman & Hall, 1994.

[16] J. P. Nolan, "Multivariate elliptically contoured stable distributions: theory and estimation," *Computational Stat.*, vol. 28, no. 5, pp. 2067–2089, 2013.

[17] ——, *Stable Distributions - Models for Heavy Tailed Data*. Boston: Birkhauser, 2015, in progress, Chapter 1 online at. [Online]. Available: http://fs2.american.edu/jpnolan/www/stable/stable.html

[18] A. Mahmood and M. Chitre, "Generating random variates for stable sub-Gaussian processes with memory," *Signal Process.*, vol. 131, pp. 271 – 279, 2017.

[19] H. S. Dol, P. Casari, T. van der Zwan, and R. Otnes, "Software-defined underwater acoustic modems: Historical review and the nilus approach," *IEEE J. Ocean. Eng.*, vol. 42, no. 3, pp. 722–737, July 2017.

[20] A. Mahmood, M. Chitre, and H. Vishnu, "Spatial ambient noise inversion using a single hydrophone," in *MTS/IEEE Oceans - Anchorage*, Sept 2017, pp. 1–6.